Available online at www.sciencedirect.com
SCIENCE DIRECT®
Ocean Modelling 6 (2004) 101–124
Ocean Modelling
www.elsevier.com/locate/omodol

On the effect of surface gravity waves on mixing in the oceanic mixed layer

Lakshmi H. Kantha [a,*], Carol Anne Clayson [b]

[a] Department of Aerospace Engineering Sciences, University of Colorado, Boulder, CO, USA
[b] Department of Meteorology, Florida State University, Tallahassee, FL, USA

Received 9 May 2001; received in revised form 8 November 2002; accepted 5 December 2002

Abstract

We apply a one-dimensional mixed layer model, based on second moment closure of turbulence, to study the effects of surface gravity waves on mixing in the oceanic mixed layer. The turbulent kinetic energy injected near the surface by breaking waves, and the kinetic energy input from Langmuir circulations that may exist in the presence of surface gravity waves, are both parameterized and included in the turbulence model. As expected, the wave breaking elevates both the turbulent kinetic energy and its dissipation rate in the upper few meters, well above the classical values expected from similarity theory for shear layers adjacent to a boundary. While there is a significant impact on mixed layer properties near the surface, wave breaking-induced turbulence decays rapidly with distance from the surface and hence the overall effects on the mixed layer are small. On the other hand, the energy input to turbulence from Langmuir cells elevates the turbulent kinetic energy and mixing throughout the mixed layer, and is therefore more effective in deepening the mixed layer. While the changes in sea surface temperature (SST) brought about by the inclusion of Langmuir cells are rather small on diurnal time scales, they can be appreciable over seasonal time scales. Nevertheless, these SST changes are well within the uncertainties in the modeled SST resulting from an imperfect knowledge of the air–sea fluxes used to drive the mixed layer models.

1. Introduction

The air–sea interface acts as a significant barrier to the exchange of heat and gases between the ocean and the atmosphere, because the transfer of these scalar quantities is mediated by molecular sublayers at the air–sea interface and the associated molecular diffusion. However, the sea surface

* Corresponding author.
E-mail addresses: kantha@colorado.edu (L.H. Kantha), clayson@fsu.edu (C. Anne Clayson).

1463-5003/$ - see front matter
doi:10.1016/S1463-5003(02)00062-8

is invariably covered with surface waves and under certain conditions, these waves break. When they do, additional transfer mechanisms come into play that are more efficient in effecting the transfer across the interface. For example, breaking waves entrain air in the form of small bubbles that are propelled into the water to depths of the order of the depth of breaking and therefore more efficiently transfer properties to the water. Similarly, spray and droplets ejected into the air during breaking are an efficient mechanism for transferring water vapor, heat and dissolved gases from the ocean to the atmosphere. Breaking waves also create additional turbulence and mixing. This has a considerable effect on the near-surface distributions of mixed layer (ML) properties, such as the velocity, temperature, salinity and concentrations of suspended matter, phytoplankton and dissolved gases. This aspect is of particular importance to air–sea exchange of green-house-active photochemicals in the water column such as carbonyl sulphide. These chemicals are produced principally in the upper few meters by the ultraviolet component of the solar insolation penetrating into the water column, and are then mixed downward by turbulent eddies in the ML. For all these reasons, it is important to include the effect of wave breaking in modeling the upper layers of the oceanic mixed layer (OML).

Surface waves are also responsible for generating large-scale coherent motions in the upper layers. These take the form of counter-rotating horizontal cells with horizontal dimensions scaling roughly with the depth of the ML and with their axes roughly aligned with the wind. These Langmuir cells have the capability to transport suspended matter such as phytoplankton and zooplankton vertically downward deep into the ML and otherwise modifying the circulation and turbulence characteristics in the upper layers. The near-surface vertical velocities in the convergence and divergence zones of these cells can reach values of the order of 10 $\mathrm{cm\,s^{-1}}$ and therefore Langmuir circulation, when present, can have a dramatic effect on near-surface properties in the ML. These cells can also transfer some of their kinetic energy directly to turbulence and this should be taken into account in ML models.

Surface waves can also extract energy from mean motions (Phillips, 1977). They can also transfer energy directly to turbulence, without any breaking (Kitaigorodskii et al., 1983). These wave–mean flow-turbulence interactions are not very well understood at present, but could nevertheless be important to the overall dynamics of the upper layers of the ocean.

Traditionally, most OML models have been patterned after the atmospheric boundary layer models (for example, Mellor and Yamada, 1974, 1982; Kantha and Clayson, 1994; Large et al., 1994), and have therefore ignored the fact that the air–sea interface is a non-rigid, mobile surface capable of sustaining gravity wave motions with all their attendant complex dynamics. The net result is that traditional concepts such as the Karman–Prandtl law of the wall in shear flows adjacent to a rigid boundary have been assumed to be valid near the more complex air–sea interface as well. In the presence of a vigorous sea state the principal balance in the turbulent kinetic energy (TKE) equation in the immediate vicinity of the air–sea interface is not between local shear production and dissipation, but is instead between downward diffusion of turbulence produced by breaking waves and dissipation. The influence of coherent motions such as Langmuir cells are also excluded in this approach. Whatever limited comparisons with observational data that have been possible (see for example, Mellor and Yamada, 1982; Kantha and Clayson, 1994; Large et al., 1994; Clayson et al., 1997) have generally supported this approach. Nevertheless, one particular situation where this approach is particularly uncomfortable is that of shallow ML such as the diurnal ML generated by weak winds and strong solar insolation and rain-ML generated by

heavy precipitation. These MLs are typically less than 10 m deep, and therefore in the presence of a vigorous sea state, gravity wave influence cannot be justifiably ignored.

There have been a few attempts to incorporate the effect of wave-breaking in ML models. Some bulk ML models (see for example, Niiler and Kraus, 1977) have recognized the fact that a mixed layer is mixed from both the top and the bottom, and in addition to incorporating the shear-produced TKE at the ML base, have parameterized the TKE input at the surface by a term proportional to u_*^3, where u_* is the water-side friction velocity. On the other hand, but for a few exceptions, second moment closure-based models (for example, Mellor and Yamada, 1982, Kantha and Clayson, 1994), have traditionally ignored this input. Those that have (Kundu, 1980; Kantha, 1988; Craig and Banner, 1994; Stacey and Pond, 1997; D'Alessio et al., 1998; Burchard, 2001) have confirmed the notion that the influence of this input is confined to the near-surface layers of the order of a few meters. All but one (Kantha, 1988) of these assume that the wave field is fully developed and corresponds to that generated by the local wind, and parameterize the TKE input at the surface as proportional to u_*^3. While the capillary-gravity range of the wind-wave spectrum adjusts rather quickly to changes in magnitude and direction of local winds, this is not generally true for the low wave number range especially near the spectral peak. Fetch effects may therefore be important and could account for the large scatter in the observed near-surface dissipation rate (see Figs. 7 and 8 of Craig and Banner, 1994).

Using large eddy simulations (LES), Skyllingstad and Denbo (1995) and McWilliams et al. (1997) have explored the impact of Langmuir cells on the turbulence in the OML. Both find elevated TKE and dissipation of TKE in the OML due to Langmuir circulation. This suggests that these effects should be included in OML models. However, while it is straightforward to simulate Langmuir cells in an LES approach, it is not clear how to parameterize their effects in a conventional ML model. Since the resource-intensive nature of LES models makes it difficult to incorporate them into complex general circulation models, it is imperative that some progress be made in parameterizing Langmuir cells in conventional ML models of the bulk and second moment closure type. We are aware of only one attempt to include the effect of Langmuir circulations in 1-D ML models; D'Alessio et al. (1998) have parameterized the energy input from Langmuir cells to TKE based on Skyllingstad and Denbo's (1995) LES results, and have also included wave-breaking effects. However, their model suffers from errors in Skyllingstad and Denbo LES formulation. Also, unlike two-equation models of turbulence (for example, Mellor and Yamada, 1982; Kantha and Clayson, 1994), where both TKE and a quantity involving the length scale are computed using prognostic equations, D'Alessio et al. (1998) prescribe the turbulence length scale using the Blackadar formulation. This paper is an attempt to parameterize the effects of wave-breaking and Langmuir circulation on turbulence in the OML, using the Kantha and Clayson (1994) two-equation second moment closure model and concentrating on the injection of TKE into the OML by these processes.

2. Wave breaking

In the past, the dearth and difficulty of measurements close to the air–sea interface, especially at high wind speeds, and reliance on observations at deeper levels tended to reinforce the traditional view that the law of the wall prevails near the interface. Extensive tower-based measurements

during the Water Air Vertical Exchange Studies (WAVES) project in the second half of 1980's (Agarwal et al., 1992; Drennan et al., 1992, 1996; Terray et al., 1996), and other observations using vertical profilers (Anis and Moum, 1992, 1995) and from a submarine (Osborn et al., 1992) have demonstrated the existence of a region of very high dissipation rate in layers adjacent to the air–sea interface that is of profound importance to matters related to mixing in the upper layers and air–sea exchanges. The dissipation rate in these upper layers is one to two orders of magnitude larger than expected from the law of the wall scaling arguments:

$$\frac{\varepsilon z}{u_*^3} = \frac{1}{\kappa} \tag{2.1}$$

where ε is the dissipation rate, u_* is the water side friction velocity, κ is the von Karman constant and z is the distance from the surface. This is due to the presence of breaking waves and their influence on a shallow layer with a depth of the order of the wave height.

Laboratory measurements of Rapp and Melville (1990) also show enhanced dissipation levels due to surface wave breaking. These observations (Melville, 1994) show that more than 90% of the energy lost due to breaking is lost quite quickly, within about four wave periods, with the breaking event itself lasting approximately a wave period, and more than 50% of the energy loss is expended in entraining air bubbles against the action of gravitational forces. The bulk of the dissipation takes place in a layer of depth of the order of the height of the breaking wave and not its wavelength. After four wave periods, the dissipative layer is 1–2 wave heights thick, but even after 100 wave periods, its depth is still of the order of the wave height. This suggests that the influence of wave breaking in elevating the dissipation rate in the upper ocean is normally confined to a layer few meters thick near the air–sea interface.

Gargett (1989) found that the dissipation rate in the upper layers of the ocean decayed as z^{-4}. This decay law is similar to that due to turbulence created by a stirring grid (Hopfinger and Toly, 1976), which can be characterized by a turbulence velocity scale $q \sim z^{-1}$, and a turbulence length scale $\ell \sim z$, where z is the distance from the grid, so that the dissipation rate $\varepsilon \sim q^3/\ell \sim z^{-4}$, and the eddy viscosity ($\sim q\ell$) is constant. Thus there is a rapid decay of TKE ($\sim z^{-2}$) in this layer and therefore its contribution to mixing in the bulk of the OML and hence to its deepening may not be very significant, unless the OML is rather shallow. The presence of this layer of elevated turbulence and dissipation rate is, however, quite important to air–sea exchanges.

Craig and Banner (1994) used second moment closure to simulate turbulence generated by breaking waves and found a $z^{-3.4}$ power law dependence for dissipation rate. Anis and Moum (1992) found a z^{-3} dependence in their microstructure measurements. Drennan et al. (1996) find z^{-2} dependence in ship observations during SWADE consistent with the WAVES tower observations of Terray et al. (1996). Thus there is considerable disagreement as to the exact value for the exponent of the power law and it is not clear at this point what the decay rate should be, although analytical considerations suggest an exponent of −4. Sufficiently far away from the wall, one recovers the law of the wall scaling. This depth at which the law of the wall is attained can be as large as 8–10 m for a very mature sea (wave age $\sim$ 26), consistent with the observations of Anis and Moum (1992) and Osborn et al. (1992). Immediately adjacent to the wall, for values of z less than about 0.6 H_s, where H_s is the significant wave height, the dissipation rate is approximately constant.

3. Langmuir cells

Langmuir (1938) was the first to observe and study the phenomena of organized counter-rotating vortices with axes aligned roughly with the wind at the surface of a lake and associated with a three-dimensional, cell-like circulation. These cells are now known as Langmuir cells or windrows. Their presence is manifest by the surface convergence at the boundary of counter-rotating cells. Windrows are often visible to the naked eye because seaweed and flotsam accumulate at the surface in these convergence regions. On a blustery day with a vigorous surface wave field, the convergence region is made visible by whitecapping and bubble entrainment due to breaking of small-scale waves in the convergence regions, resulting in parallel white lines roughly aligned with the wind and roughly uniformly spaced. Langmuir carried out a series of observations confirming the existence of cell-like circulation associated with windrows.

Langmuir cells are also associated with the bubble clouds (Thorpe, 1984; Farmer and Li, 1995) seen in side-scan sodar observations of the near-surface layers of the ocean (Thorpe, 1992). The bubble plumes are manifest in the form of streaks with a variety of scales, merging at characteristic Y junctions to form large circulation cells, with the streaks aligned in the wind direction and drifting to the right of the wind. These bubble plumes are concentrated at surface convergence zones. Bubble clouds are important to air–sea gas transfer, and because they are efficient volume backscatterers, important also to ocean acoustics at high frequencies. The depth of penetration of the bubble cloud depends very much on the strength of the surface convergence and hence the strength of Langmuir circulations.

It has long been suspected that Langmuir cells might play a role in the mixing in the upper ocean, and other near-surface processes such as air–sea exchange of gases, entrainment of bubbles, photochemical production in the upper layers, and vertical transfer of momentum and other properties into the interior from the air–sea interface. This is simply because these cells can be quite vigorous and the downward vertical velocity immediately below the convergence region can be as high as a few tens of cm s^{-1}, leading to bubble entrainment and transport to greater depths. The cells also provide a mechanism for distribution of properties in the vertical in the ML and transport of phytoplankton and zooplankton in the vertical. However, their intimate association with the surface wave field makes Langmuir cells inherently transient events, hard to observe and measure. Consequently, not much is known about their generation and decay characteristics, and it has been difficult to assess their importance and significance. Leibovich (1983) (see also Pollard, 1977) has reviewed earlier work on Langmuir cells. Weller and Price (1988) found that Langmuir cells were able to rapidly destroy the surface thermal stratification in shallow diurnal MLs. The vertical velocities below the convergence zones, while quite strong immediately below the surface, also decay rapidly with depth. Thus, Langmuir cells are undoubtedly important to mixing in the OML.

In the modeling arena, Skyllingstad and Denbo (1995) were the first to perform LES simulations of Langmuir circulations under a variety of conditions, including wind- and convection-driven mixing with and without Stokes drift to highlight their importance in the structure of the upper layers. The enhancement of vertical velocity variance and the increased entrainment heat flux led to their conclusion that Langmuir circulations might be important to the dynamics of the OML. However, they ignored the modification of the Coriolis and pressure terms in the mean momentum equation by Stokes drift. McWilliams et al. (1997) have corrected this oversight and

demonstrated the changes in the mean and turbulence fields brought about by the presence of Langmuir circulation.

Langmuir circulations (Craik and Leibovich, 1976) are formed due to the interaction of the wind-driven surface shear with the Stokes drift of the surface waves. The governing momentum equations are modified by the appearance of a vortex force term as well as modification of Coriolis term by the Stokes drift. Neglecting viscous terms for simplicity, the governing equations for momentum can be written as (see McWilliams et al., 1997)

$$\frac{\partial U_{\mathrm{j}}}{\partial t}+\frac{\partial}{\partial x_k}(U_{\mathrm{k}}U_j)+\varepsilon_{jkl}f_k(U_1+V_{\mathrm{S}l})=-\frac{1}{\rho_0}\frac{\partial \Pi}{\partial x_j}-g_j\beta\Theta-\frac{\partial}{\partial x_k}(\overline{u_k u_j})+\varepsilon_{jpl}V_{\mathrm{S}p}\Omega_1 \tag{3.1}$$

where $\Omega_l=\varepsilon_{lmn}\dfrac{\partial U_n}{\partial x_m}$ is the vorticity and Π is the generalized pressure that includes the contribution from the

$$\text{Stokes drift}: \quad \Pi=p+\frac{\rho_0}{2}[(U_i+V_{\mathrm{S}i})(U_i+V_{\mathrm{S}i})-V_{\mathrm{S}i}V_{\mathrm{S}i}] \tag{3.2}$$

The quantity $V_{\mathrm{S}i}$ (note that $V_{\mathrm{S}3}=0$) is the Stokes drift velocity due to surface waves, whose magnitude is given by

$$|V_{\mathrm{S}}|=(V_{\mathrm{S}i}V_{\mathrm{S}i})^{1/2}=V_{\mathrm{S}0}\exp(2kz)=c(ka)^2\exp(2kz) \tag{3.3}$$

where c is the wave phase speed, k is the wave number and a is the amplitude. This vortex force acts like a buoyancy force term in the vertical momentum equation.

The horizontally averaged KE equation for the resolved scales in LES can be written as

$$\frac{\partial}{\partial t}q^2=-2\overline{u_k u_j}\frac{\partial U_j}{\partial x_k}-2\overline{u_3 u_j}\frac{\partial V_{\mathrm{S}j}}{\partial x_3}+\cdots \tag{3.4}$$

where only the traditional Reynolds stress production term and the Stokes drift term are retained for simplicity. The most important thing to note is the appearance of the production term due to the Stokes drift. When the cells are fully developed, one can expect that this energy input is lost to small-scale turbulence and hence act as an additional source term in the TKE equation.

The appropriate velocity scale for Langmuir circulations may be taken as (Kantha and Clayson, 2000):

$$V_{\mathrm{L}}\sim(u_*^2V_{\mathrm{S}0}\cos\theta)^{1/3}\sim[u_*^2(\mathrm{ka})^2C\cos\theta]^{1/3} \tag{3.5}$$

where θ is the angle between the shear stress and the Stokes drift vectors. Eq. (3.5) suggests that the strength of the Langmuir circulations depends on the combined effects of the Stokes drift and wind stress, so that strong winds and small waves can have an influence similar to that of weak winds and large waves. But both are essential. This fact is underscored by Plueddemann et al. (1996), who could not scale their sonar observations of the near-surface rms convergent velocities during Surface Wave Processes Program (SWAPP, Weller et al., 1991) by the friction velocity alone and had to use a velocity scale based on the combination of the friction and Stokes velocities. They, however, used $(u_*V_{\mathrm{S}0})^{1/2}$ as the characteristic velocity scale for Langmuir circulations.

Skyllingstad and Denbo (1995) failed to include the Stokes drift contribution to the Coriolis term in Eq. (3.1) and the pressure term in Eq. (3.2). They also derived a TKE equation similar to Eq. (3.4), but the form is different since they did not include the Stokes term in the generalized

pressure. D'Alessio et al. (1998) have used the Skyllingstad and Denbo form of the TKE input to parameterize the impact of Langmuir cells on mixing in the OML.

McWilliams et al. (1997) present solutions for a laminar Ekman layer in the presence of Stokes drift and show how the laminar Ekman profile is modified by the Stokes drift to yield an angle between the wind direction and the surface velocity larger than the 45° value typical of the classic laminar Ekman layer. They also performed LES calculations for the case of a monochromatic surface wave of 60 m wavelength (wave number $k = 0.105\ \mathrm{m}^{-1}$) and 0.8 m amplitude (providing a Stokes drift V_S of $0.068\ \mathrm{m\,s}^{-1}$) in the presence of a $5\ \mathrm{m\,s}^{-1}$ wind blowing over the surface (providing u_* of $0.0061\ \mathrm{m\,s}^{-1}$), so that the Langmuir number La equal to $(u* \ /V_S)^{1/2}$ is 0.3. The latitude of the ML was 45°, with the inversion at a depth of 33 m, so that $kd = 3.465$, where d is the ML depth. This situation corresponds to a strongly sheared PBL, where Langmuir effects can be expected to be significant. Their calculations show elevated TKE and dissipation rate of TKE in the ML, especially the upper part, as well as a significant increase in eddy viscosity. The velocity profiles in the Ekman layer were also more uniform than in the case without Langmuir circulations. It is important to note that both La and kd are important non-dimensional parameters in the problem, the first one signifying the relative strength of the Stokes drift, and the second, its relative depth of penetration.

4. The mixed layer model–the length scale equation

The ML model we will use (Kantha and Clayson, 1994) is based on the Mellor–Yamada (MY henceforth) type second moment turbulence closure (Mellor and Yamada, 1982; Galperin et al., 1988). Here, the second moment equations are reduced to a single equation for q^2 (twice the TKE) and algebraic relations for the second moments. In addition, since the minimum description of turbulence must consist of two quantities, its velocity scale (indicative of the energy contained in turbulent fluctuations) and its length scale (indicative of the scale of the energy containing eddies), the turbulence macroscale ℓ is either prescribed or derived through a conservation equation for $q^2\ell$. It is here that other closure models differ; for example, one popular model uses a conservation equation for the dissipation rate of TKE (ε) to provide information on the length scale. Since $\varepsilon \sim q^3/\ell$ for high Reynolds number turbulence, this is a surrogate equation for ℓ. There are other conservation equations possible, for example for the quantity $q\ell$ (indicative of the eddy viscosity) and q/ℓ (indicative of the turbulence frequency–frequency pertaining to energy containing eddies). Unlike the TKE equation which has a firm physical basis, and which all these closure models use, the equation for the length scale, no matter which quantity is used, is merely patterned after the TKE equation and consequently, its physical basis is tenuous (Kantha, 1988). Both these equations contain a production and a destruction term, as well as a diffusion term; unfortunately, unlike in the TKE equation, in the length scale equation, all these terms have to be modeled, and herein lies a major difficulty in two-equation turbulence models of this type.

While there is no ambiguity in the form of the q^2 equation, which can be written as (Mellor and Yamada, 1982; Galperin et al., 1988; Kantha and Clayson, 1994)

$$\frac{\mathrm{D}}{\mathrm{D}t}(q^2) - \frac{\partial}{\partial z}\left[q\ell S_q \frac{\partial}{\partial z}(q^2)\right] = -2\left(\overline{uw}\frac{\partial U}{\partial z} + \overline{vw}\frac{\partial V}{\partial z}\right) + 2\beta g\overline{w\theta} - 2\frac{q^3}{B_1\ell} \tag{4.1}$$

the most general form for the $q^2\ell$ equation (Kantha et al., 1989; Kantha and Rosati, 1990) is

$$\frac{\mathrm{D}}{\mathrm{D}t}(q^2\ell) - \frac{\partial}{\partial z}\left[q\ell S_1 \frac{\partial}{\partial z}(q^2\ell)\right] = E_1\ell\left(-\overline{uw}\frac{\partial U}{\partial z} - \overline{vw}\frac{\partial V}{\partial z}\right) + E_3(\beta g\overline{w\theta}) - E_2\frac{q^3}{B_1}\left[1 + E_4\left(\frac{\ell}{\kappa\ell_w}\right)^2\right] + E_5(2\Omega)q^2\ell \tag{4.2}$$

The last term accounts for the effect of rotation (Ω is the rotation rate of the reference frame), important only in strongly rotating flows, and therefore, usually ignored in most geophysical flows. The first three terms on the right-hand side of Eqs. (4.1) and (4.2) denote shear production, buoyancy production (destruction) and dissipation, respectively. Note that in addition to the production, destruction and diffusion terms, a wall-proximity term indicated by the very last term is somewhat arbitrarily added to the $q^2\ell$ equation to force a log-law behavior near a bounding surface (ℓ_w is the distance from the surface). The second term on the left-hand side of Eqs. (4.1) and (4.2) represents down-the-gradient diffusion, and parameters S_q and S_1 are eddy diffusion coefficients.

So far very little attention has been paid to the performance of the $q^2\ell$ equation in MY type models. Specifically, there is considerable uncertainty as to the precise values of the universal constants in this equation. Based on a limited amount of relevant data, Mellor and Yamada (1982) recommended $S_q = S_1 = 0.2,\ E_1 = 1.8,\ E_2 = 1,\ E_3 = 1.8,\ E_4 = 1.33,\ E_5 = 0$, and these values have been used ever since in most MY type closure, although a value of $S_q = S_1 = 0.41$ is more common, to assure adequate diffusion. Kantha et al. (1989) recommended $E_5 = 0.04$. In particular, to insure that as $\ell \to \kappa z$ as $z \to 0$, E_1 and E_4 cannot be chosen independently and are related to each other. It can also be shown (Kantha, 1988; see also Burchard and Deleersnijder, 2001) that by choosing a value of E_3 greater than unity (~5–9) under stable stratification conditions, it is possible to avoid imposing an additional constraint on the length scale based on Ozmidov length scale considerations (Kantha and Clayson, 1994; Galperin et al., 1988): $N\ell/q < 0.53$.

There are also indications, notwithstanding statements to the contrary by Mellor and Yamada (1982) that the diffusion coefficient S_1 must be greater than S_q. This latter fact is quite important. In the TKE equation, compared to the production and destruction terms, the diffusion term plays a very minor role (this is one reason why the down-the-gradient model for the diffusion term, while clearly inaccurate, does not appear to seriously affect the model performance), and in most practical situations, the turbulence is in near-equilibrium, where the production and destruction terms closely balance each other. On the other hand, the diffusion term in the $q^2\ell$ equation is as important as the production and dissipation terms, and care must be given to the proper choice of S_1. While the performance of MY type models in applications to the OML does not appear to have suffered due to these deficiencies, it is clearly time to reexamine the length scale equation, especially in the present context.

In the wave-mixed upper oceanic mixed layer, energy injection by breaking surface waves is accompanied by shear production of TKE deeper below. Mixed layer models have traditionally been tuned to perform well for the latter situation, but not the former, where the turbulence is dominated by diffusion away from the source. A popular analog to wave-mixing is the turbulence generated by a stirring grid that has been extensively studied by turbulence researchers.

Unfortunately, experiments with stirring grids suffer from a variety of problems (including wall effects, residual mean circulation, not high enough Reynolds numbers and finite oscillation amplitude etc.) and the precise power law for the decay of TKE with distance from the source is uncertain. Dimensional considerations dictate that the length scale must scale as the distance from the source ($\ell \sim z$), but the value of $2m$ in $q^2 \sim z^{-2m}$ is quite uncertain. The situation here is somewhat analogous to decaying turbulence behind a grid in a wind tunnel, where theory dictates $q \sim t^{-1}$ in the ideal situation of infinite Reynolds number turbulence, while experimental values suggest a non-unity exponent in the necessarily non-ideal experimental setups. Nevertheless, there are indications that $q \sim z^{-1}$ so that the dissipation rate $\varepsilon \sim z^{-4}$ and turbulent viscosity $\nu_t \sim$ constant. Eqs. (4.1) and (4.2) must reproduce this behavior.

In the neutrally stratified log-layer, by simple dimensional reasoning, $\ell = \kappa z$, $\mathrm{d}U/\mathrm{d}z = u_*/\kappa z$, and $q = B_1^{1/3} u_*$. Substituting these values and neglecting tendency and buoyancy terms, it is possible to show that q^2 equation (4.1) is identically satisfied, irrespective of the value of S_q, since the diffusion terms are identically zero. Doing the same for the $q^2\ell$ equation, Eq. (4.2) is satisfied provided

$$B_1 \kappa^2 S_1 = E_2(E_4 + 1) - E_1 \tag{4.3}$$

Note that S_1 appears because, unlike the q^2 equation, the diffusion term in the $q^2\ell$ equation is non-zero even in the log-layer.

For the stirring grid case, $q = az^{-m}$, $\ell = bz$, $\mathrm{d}U/dz = 0$. Note that $m \sim 1$, and there is no apriori reason to assume that b must be equal to κ (in fact κ is defined as the proportionality constant in the $\ell \sim z$ relationship in the logarithmic region of a neutrally stratified boundary layer adjacent to a solid surface, and this has nothing to do with decaying turbulence behind a grid or for that matter turbulence generated by wave breaking). Neglecting once again the tendency and buoyancy terms (production term is identically zero), Eqs. (4.1) and (4.2) give

$$3B_1 b^2 S_q = \frac{1}{m^2} \tag{4.4}$$

$$B_1 b^2 S_1 = \frac{E_2[E_4 + (b/\kappa)^2]}{(2m-1)(3m-1)} \tag{4.5}$$

Eqs. (4.3)–(4.5) can be rewritten as

$$\begin{aligned} E_4 &= \frac{(2m-1)(3m-1)}{m(6m-5)}\left(\frac{E_1}{E_2} - 1\right) + \frac{\left(\frac{\kappa}{b}\right)^2}{m(6m-5)} \\ \frac{S_1}{S_q} &= \frac{E_2(E_4+1) - E_1}{B_1 \kappa^2 S_q} \\ \left(\frac{\kappa}{b}\right) &= m(3B_1 \kappa^2 S_q)^{1/2} \end{aligned} \tag{4.6}$$

There is little reason to change the value of S_q or E_1, which have worked well so far in MY models. Also note that m must be greater than 5/6 to assure positive values for E_4. Based on this and the considerations mentioned above, we choose $m = 1$. Thus the value of κ/b is immediately fixed: 1.81. Choosing the traditional value for E_2 of 1.0 yields $E_4 = 4.88$ (note the traditional MY

value is 1.33) and $S_1/S_q = 3.74$ (traditional value is 1). For the time being, we will fix the value of E_3 at 1.0 and impose the buoyancy constraint on the length scale in stably stratified flows.

We include the effects of Langmuir circulation in this model by modifying Eqs. (4.1) and (4.2) to account for the additional turbulence production terms:

$$\frac{\mathrm{D}}{\mathrm{D}t}(q^2) - \frac{\partial}{\partial z}\left[q\ell S_q \frac{\partial}{\partial z}(q^2)\right] = -2\overline{uw}\left(\frac{\partial U}{\partial z} + \frac{\partial u_S}{\partial z}\right) - 2\overline{vw}\left(\frac{\partial V}{\partial z} + \frac{\partial v_S}{\partial z}\right) + 2\beta g\overline{w\theta} - 2\frac{q^3}{B_1\ell} \tag{4.7}$$

$$\frac{\mathrm{D}}{\mathrm{D}t}(q^2\ell) - \frac{\partial}{\partial z}\left[q\ell S_1 \frac{\partial}{\partial z}(q^2\ell)\right] = E_1\ell\left(-\overline{uw}\frac{\partial U}{\partial z} - \overline{vw}\frac{\partial V}{\partial z}\right) + E_6\ell\left(-\overline{uw}\frac{\partial u_S}{\partial z} - \overline{vw}\frac{\partial v_S}{\partial z}\right) + E_3(\beta g\overline{w\theta}) - E_2\frac{q^3}{B_1}\left[1 + E_4\left(\frac{\ell}{\kappa\ell_w}\right)^2\right] + E_5(2\Omega)q^2\ell \tag{4.8}$$

where u_S and v_S are components of the Stokes drift velocity V_S. The new model constant introduced into the mixing model, E_6, has to be chosen greater than unity to simulate the vigorous mixing produced by Langmuir cells. Its value can only be determined empirically. We have therefore simulated the McWilliams et al. (1997) monochromatic surface wave case with the Langmuir number La of 0.3. Fig. 1 shows the model results with and without the Langmuir circulation terms in Eqs. (4.7) and (4.8). The modeled increases in TKE and its dissipation rate in the bulk of the ML due to Langmuir circulation are of very similar magnitude to that of McWilliams et al. (their Figs. 4 and 5). The increase in the mixing coefficient K_M, however, depends on the value of E_6. With $E_6 = 1$, the K_M values are only slightly higher than that for the case without Langmuir terms, even though the TKE and dissipation levels do agree well with the LES results (see the middle panel in Fig. 1). But for $E_6 \sim 4$, the increase in the mixing coefficient is of similar magnitude to that in McWilliams et al. (1997) simulations (their Fig. 3). We therefore

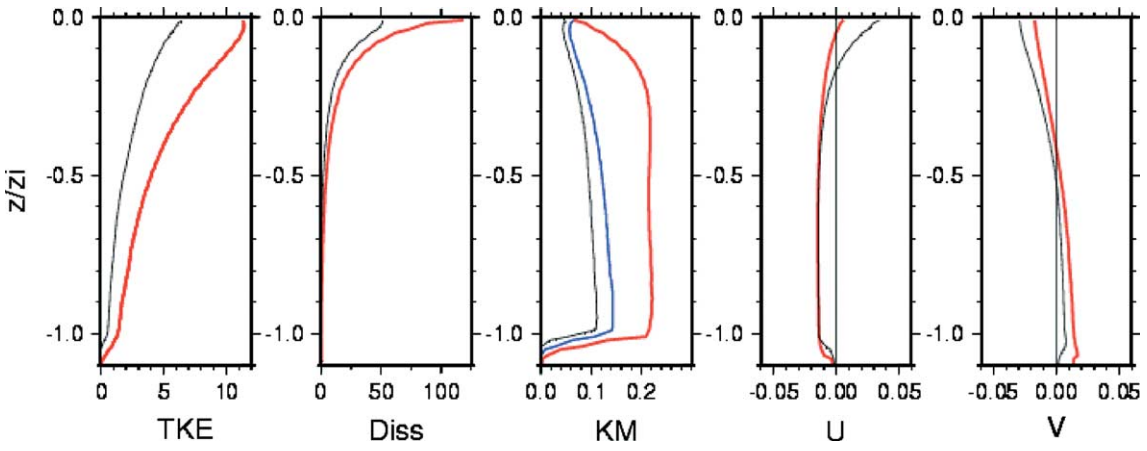

Fig. 1. Model results at 45° latitude without (thin black line) and with (thick red line) turbulence injection from Langmuir cells for conditions identical to the McWilliams et al. (1997) LES calculations. The panels show from left to right, TKE normalized by u_*^2, dissipation rate of TKE normalized by u_*^2/z_i, the eddy viscosity K_M normalized by u_*z_i, the u component of velocity in m s^{-1} and the v component of velocity in m s^{-1}. Quantity u_* is the water-side friction velocity and z_i is the inversion depth (see McWilliams et al., 1997 for details). The medium blue line in the center panel indicates the K_M values when the model constant E_6 is put equal to unity.

choose a value of 4 for E_6, a new model parameter. It is important to note that a value for E_6 much higher than unity is crucial, since it enables the turbulence length scale (and hence the mixing) in the mixed layer to be increased significantly in the presence of Langmuir cells, which is consistent with the fact that these cells are indeed large scale structures.

Fig. 1 also shows the velocity profiles from the model. Both u and v velocity profiles are not as uniform as in McWilliams et al. calculations, even though the trends are very much similar. In particular, while the u- and v-components decrease in the upper layers when Langmuir effects are included, they do not decrease as much as theirs (their Fig. 2). This suggests that while we may have successfully included one rather important aspect of Langmuir circulation in the 1-D model, namely its turbulence injection into the ML, we may have not managed to capture all its effects, notably its subtle effects on momentum transfer in the mixed layer, which leads to somewhat flatter velocity profiles. Nevertheless, these simulations are quite striking.

It is important to note here that in one-equation turbulence models, where TKE is determined by a prognostic equation such as Eq. (4.7) but the turbulence length scale is arbitrarily prescribed (and not calculated), it is necessary to guess the correct form for the variation of length scale in the ML. This is hard to do except under some rather simple circumstances. For more general applications, the changes in the length scale brought about by effects such as those due to Langmuir cells, are best simulated with a two-equation turbulence model, even though it is computationally more expensive.

5. Turbulence input from wave motions

Parameterizing the TKE input at the surface by wave breaking at limited fetches requires a knowledge of the wind wave spectrum. Starting with the pioneering effort by Phillips (1958), considerable effort has gone into determining the shape of the wind–wave spectrum. Phillips (1958) hypothesized a saturation range in the high wavenumber range of the spectrum, where the waves are saturated and therefore any energy input by the wind is immediately lost by breaking. From dimensional arguments, it is easy to show that this leads to -5 power law for the frequency spectrum

$$\Phi(n) = \alpha g^2 n^{-5} \tag{5.1}$$

where α is the Phillips constant (with a value of around 0.015), g is the gravitational acceleration, and n is the radian frequency. This hypothesis was, however, revised (Phillips, 1985, see also Kitaigorodskii, 1986) to bring the theory more into line with the empirical spectrum (for example, Toba, 1973) that consistently showed a -4 power law for the frequency spectrum beyond the spectral peak

$$\Phi(n) = \left(\frac{u^*}{c}\right)\beta g^2 n^{-5} = \beta u^* g n^{-4} \tag{5.2}$$

where β is the Toba constant (with a value of around 0.11) and u^* is the friction velocity corresponding to the air side of the interface. This corresponds to an equilibrium state of the waves where the energy input by the wind, spectral transfer of energy by resonant wave–wave interactions and wave dissipation are all in rough balance. Detailed observations however appear to indicate

the presence of both equilibrium and saturation ranges in the wind–wave spectrum (for example Forristall, 1981, Kahma, 1981 among others), which led Kitaigorodskii (1986) to suggest a composite spectrum with the equilibrium range prevailing in the vicinity of the peak of the spectrum, but saturation range at the tail end, with the transition between the two occurring at a frequency given by $n_t = (\alpha/\beta)(g/u^*)$ consistent with observations. For purposes of this paper, we will assume that the wind–wave spectrum is truncated at the low wave number end at the spectral peak n_p, and consists of the equilibrium range (5.2) from n_p to n_t and the saturation range (5.1) from n_t to ∞. Integration of the spectrum readily leads to the energy density $E_d = \rho g \overline{\zeta^2}$ from which

$$\frac{g^2\overline{\zeta^2}}{(u^*)^4} = \frac{\beta}{3}A^3 - \frac{\beta^4}{12\alpha^3} \tag{5.3}$$

where $\overline{\zeta^2}$ is the square of the wave amplitude and A is the wave age equal to c_p/u^*, where c_p is the phase speed at the spectral peak. The larger the value of A, the more developed the wave field. Following Longuet-Higgins (1969), (see also Phillips, 1977, pp. 196–197), the energy flux from breaking waves can be shown to be proportional to $n_p E_d$ and can be written as

$$\frac{E_f}{\rho(u^*)^3} = \gamma_1\left[\frac{\beta}{3}A^2 - \frac{\beta^4}{12\alpha^3 A}\right] \tag{5.4}$$

where γ_1 is an unknown constant. Wave age A is a function of the fetch. Observations (see Phillips, 1977) suggest

$$A = 0.45\left(\frac{gx}{(u^*)^2}\right)^{1/4} \tag{5.5}$$

with an upper bound on c_p roughly equal to U_{10}, the wind speed at anemometric height, so that the upper bound on A is $(c_d)^{-1/2}$, a value of roughly 26. This corresponds to a fully developed wave field. Since $u^* = u_*\sqrt{\rho_w/\rho_a} = 28.66u_*$, Eq. (5.4) can be rewritten as

$$\frac{E_f}{\rho u_*^3} = 4.053\left[0.037A^2 - \frac{3.615}{A}\right] \tag{5.6}$$

making use of the fact that Craig and Banner (1994) and Stacey and Pond (1997) have used a value of 100 for $\frac{E_f}{\rho u_*^3}$ in their simulations, which correspond to a fully developed wave field with a wave age A of $\sim$26.

When waves break, they give up some of their energy to turbulence, which is eventually dissipated. However, the associated momentum is transferred to the currents. There is however no need to include this explicitly in the model since the conventional drag coefficient encompasses the wave breaking effects as well.

The ML model can be run with either the Neumann boundary condition on TKE flux at the surface

$$K_q\frac{\partial q^2}{\partial z} = 2\frac{E_f}{\rho} \tag{5.7}$$

or the Dirichlet condition on q^2, following Kundu (1980), Kantha (1988), Craig and Banner (1994) and Stacey and Pond (1997) as given by Eq. (A.12). The latter is computationally more

convenient. Also, since McWilliams et al. (1997) LES results do show elevated TKE near the surface under the influence of Langmuir cells, we added a contribution from Langmuir cells to the TKE boundary condition at the surface: $q^2|_0 = C_1 V_L^2$, with the value of C_1 chosen to be unity. The results in the bulk of the ML are however relatively insensitive to the precise value of C_1.

The value of the Stokes drift velocity at the air–sea interface is

$$V_{S0} = \int_0^\infty \frac{n^3}{g} \Phi(n)\, dn = \beta u^* \left[1 + \ln\left(\frac{\alpha}{\beta} A\right)\right] \tag{5.8}$$

so that

$$\frac{V_{S0}}{u_*} = 28.66\beta \left[1 + \ln\left(\frac{\alpha}{\beta} A\right)\right] = 3.15[1 + \ln(0.136A)] \tag{5.9}$$

For fully developed waves, V_{S0}/u_* is 7.14. Li and Garrett (1993) recommend $V_{S0} = 0.016\ U_{10}$. Using a typical value of 0.0015 for c_d, this yields $V_{S0}/u_* = 11.8$. Since a truncated spectrum tends to underestimate the Stokes drift, we have chosen to use the Li and Garrett value for V_{S0} in our model simulations: $V_{S0} = 11.8 u_*$.

The effective wave number k_S of the Stokes drift current can be taken to correspond to the mean frequency n_m, which can be shown to be approximately $1.5 n_p$ for the truncated Toba-Phillips spectrum. The corresponding wave number $k_S = (1.5)^2 k_p$. Since $k_p = g/c_p^2$, the effective wave number

$$k_S = \left(\frac{1.5}{A}\right)^2 \frac{g}{(u^*)^2} = \frac{0.00274 g}{A^2 u_*^2} \tag{5.10}$$

For a fully developed wave field, this gives $k_S = 0.033 g/(u^*)^2$, slightly smaller than the Li and Garrett value of $k_S = 4.17 g/U_{10}^2$.

6. Model results

Model simulations have been carried out with and without wave breaking, and with and without the turbulence input from Langmuir circulations, for saturated wind–wave conditions and for a diurnal equatorial mixed layer. The wind stress is 0.037 N, corresponding to roughly a 5 $m\,s^{-1}$ wind. The Stokes drift is assumed to be 0.068 $m\,s^{-1}$ corresponding to a 0.8 m amplitude wave of 60 m wavelength (wave number $k = 0.105\ m^{-1}$). These conditions are the same as in McWilliams et al. (1997) LES. For each case, the model was run for 5 days with a half-sinusoidal SW solar flux with a peak amplitude of Q_{Sp} of 1000 $W\,m^{-2}$ and a constant net air–sea flux Q_{as} of $-200\ W\ m^{-2}$. Only the last two days of the simulation are shown. Fig. 2 shows the resulting SST for all four cases (1) without wave breaking and Langmuir cells, (2) with wave breaking only, (3) with Langmuir cells only, and (4) with both wave breaking and Langmuir cells. The SST is not very much affected by the inclusion of wave breaking, but somewhat stronger changes in SST arise from the inclusion of the Langmuir terms. Wave breaking makes a significant impact on TKE and its dissipation rate close to the surface, whereas the inclusion of Langmuir cells produces elevated TKE and dissipation rate levels throughout the mixed layer (not shown). Increased mixing

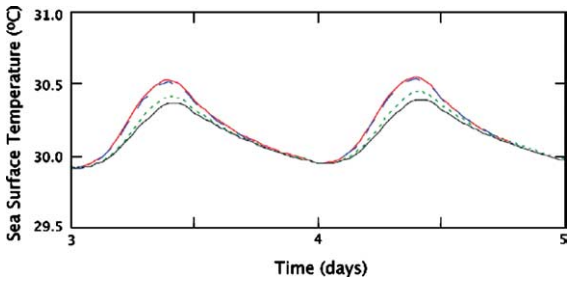

Fig. 2. SST for the equatorial ML: no wave breaking or Langmuir TKE input (solid red line); wave breaking effects included but no Langmuir terms (blue dashed line); no wave breaking effects but Langmuir terms included (dotted green line); and both wave breaking and Langmuir terms included (black solid line). The maximum temperature drop is about 0.16 °C.

deepens the ML; thus, the sea surface temperature drops in cases where the Langmuir terms are included. Nevertheless, the impact of wave breaking and Langmuir cells on SST, one of the important parameters related to the OML are rather small.

The results for mid-latitude MLs are qualitatively similar. Model runs for a diurnal ML at 45° latitude with identical forcing conditions as above produced similar results as can be seen in Fig. 3. Note that because of the slight excess of heat flux into the ML, in this case, the SST increases slowly with time. The decreased SST is due to elevated levels of TKE (Fig. 4) and hence mixing in the ML.

The impact of changes in TKE on the velocity profiles in the equatorial ML can be seen from Fig. 5, which shows the velocity profiles for all four cases. As is to be expected, increase in mixing tends to make properties more homogeneous in the water column. The increased mixing in the water column tends to decrease the velocity in the near-surface layers, with a corresponding increase in the layers below. The influence of wave breaking itself is rather small. The Langmuir generation of TKE has a relatively bigger impact, leading to more dramatic decrease of velocity in the near-surface layers and a corresponding increase in the layers below.

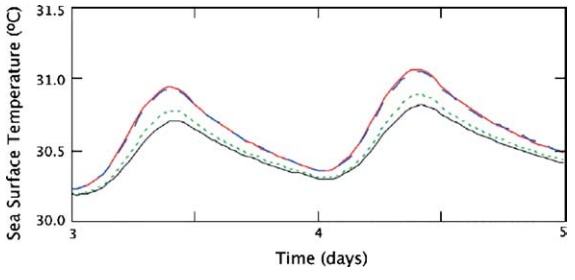

Fig. 3. SST for a mid-latitude ML: no wave breaking or Langmuir terms (solid red line); wave breaking effects included but no Langmuir terms (blue dashed line); no wave breaking effects but Langmuir terms included (dotted green line); and both wave breaking and Langmuir terms included (black solid line). The maximum temperature drop is about 0.25 °C.

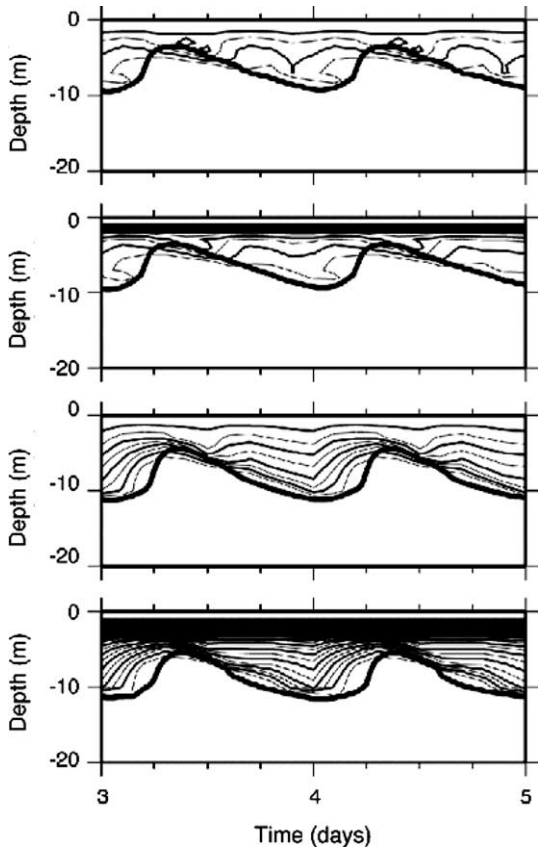

Fig. 4. TKE distribution in the mid-latitude ML (CI = 0.5 $cm^2 s^{-2}$). From top to bottom: no wave breaking or Langmuir terms; wave breaking effects included but no Langmuir terms; no wave breaking effects but Langmuir terms included; and both wave breaking and Langmuir terms included. The black line denotes the bottom of the ML. Note the elevated TKE levels near the surface from wave breaking (second and fourth panels from the top) and throughout the ML by Langmuir cells (third and fourth panels).

Most earlier ML models including wave-breaking effects have assumed the wave field to be fully developed. The energy flux from breaking waves is, however, a strong nonlinear function of fetch. To investigate this effect, we carried out simulations (not shown) for two additional wave ages: 5 and 12. However, the impact of fetch on the effect of wave breaking on SST is rather small, since the effect even for a fully developed wave field is small to begin with (Figs. 2 and 3). Therefore, the standard practice of assuming the wave field is fully developed when incorporating wave breaking effects into a ML model is quite acceptable. However, it is important to note that fetch effects may be important when the effects of Langmuir cells are considered, since the magnitude of the Stokes drift is a strong function of the wave age.

To investigate the influence of wave breaking and Langmuir cells on SST on seasonal time scales, we performed simulations of the OML at OWS Papa for the year 1961 (see Kantha and Clayson, 1994 for details), with and without wave breaking and Langmuir terms in the model.

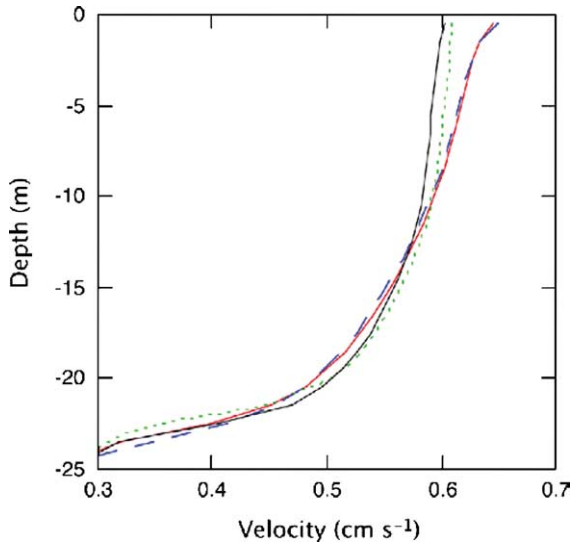

Fig. 5. Velocity profiles in the equatorial ML for four cases: with no Langmuir or wave breaking terms (red solid line), with only wave breaking included (blue dashed line), with only Langmuir terms included (green dotted line), and with both Langmuir and wave breaking terms (black solid line).

Fig. 6 shows the resulting SST and MLD for all four cases. Wave breaking does not affect the OML evolution as much as the Langmuir cells, which is not surprising. However, the inclusion of the Langmuir terms in the model tends to deepen the mixed layer significantly. The effect is largest during the spring heating cycle. The mixed layer can be deeper at times by as much as 20 m and the SST can decrease by as much as 0.5 °C. This does produce a better agreement between the model and observations during springtime, but the agreement worsens a bit during the fall cooling cycle, although towards the end of the year, the agreement improves once again. However it is important to note that similar changes in SST can result from relatively small adjustments to the prescribed radiative or surface heat fluxes, and even small changes in model parameters. Since air–sea fluxes are seldom directly measured and even if measured, not with enough accuracy, the agreement or lack of it between observed and model SSTs can be attributed either to the fluxes or to the model itself. Nevertheless, it is fair to conclude that for consistency, ML models should include at least the effect of Langmuir cells, although many ML models have successfully simulated the seasonal evolution of SST at various places (for example, Kantha and Clayson, 1994), without including either the Langmuir cell or the wave breaking effects.

D'Alessio et al. (1998) also studied the effect of Langmuir cells on mixed layer evolution at station Papa and showed that the mixed layer depth increased somewhat during winter. However, they do not show the effect on SST itself and did not do a thorough study of the Langmuir effect itself. While the results of this study are consistent with their findings in that the turbulence injection from Langmuir cells tends to deepen the mixed layer, it is important to point out that their Langmuir TKE input term, which they based on Skyllingstad and Denbo (1995) LES results, is incorrect. This study has used the correct form due to McWilliams et al. (1997) LES. They also did not use a length scale equation, preferring instead to prescribe the length scale.

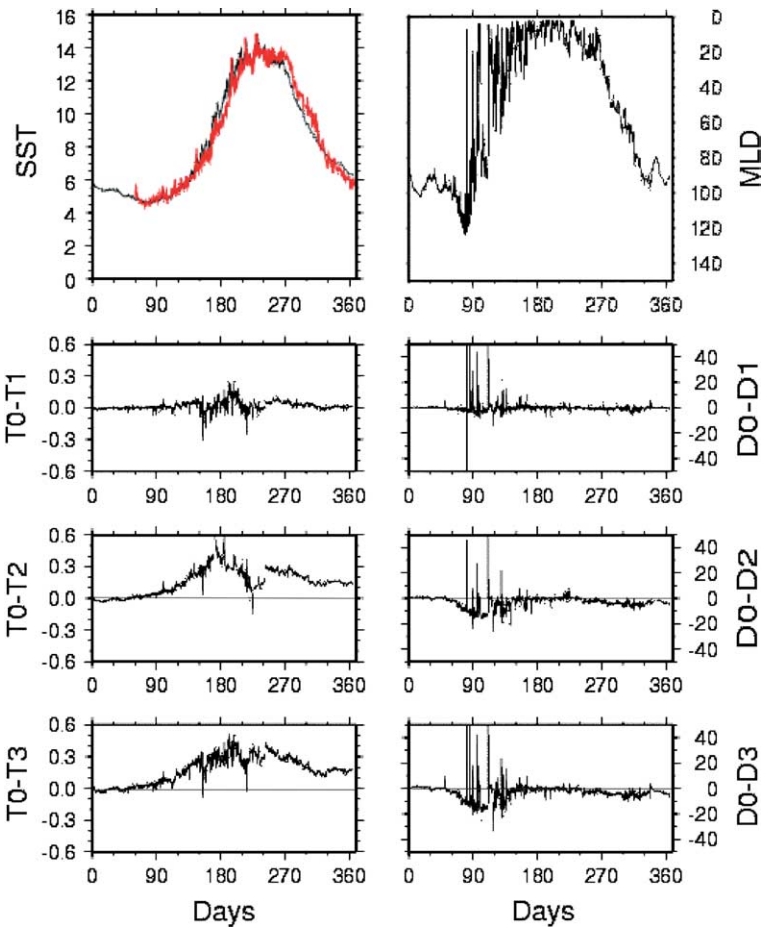

Fig. 6. Model Results for OWS Papa for the year 1961 (see Kantha and Clayson, 1994 for details). Top left hand panel shows the model SST (thin black line) compared to observed SST (thick red line) for the base case without wave breaking and Langmuir terms. The top right-hand panel shows the model MLD for the base case. The bottom three panels show the difference between the modeled SSTs (left-hand panels) and MLDs (right-hand panels): T0 and D0 are the SST and MLD for the base case; T1 and D1 for the case with wave breaking terms only; T2 and D2 for the case with Langmuir terms only; T3 and D3 for the case with both Langmuir and wave breaking terms included.

7. Concluding remarks

We have modified the second moment closure-based two-equation ML model of Kantha and Clayson (1994) to account for the injection of turbulence into the ML from wave breaking and Langmuir cells. The results show that the changes in ML properties due to wave-breaking are dramatic in the upper few meters of the OML, as expected. However, the highly dissipative nature of turbulence makes the TKE injected at the surface by wave breaking decay rapidly with depth and therefore the effect of wave breaking is confined typically to the upper few meters. Therefore, in shallow diurnal MLs, typically several meters deep, the effects of wave breaking on the upper level turbulence (to a lesser extent, on the sea surface temperature) can be expected to be

significant. However, for MLs deeper than 20–30 m, the impact of wave breaking on the overall ML dynamics can be expected to be small. Nevertheless, where near-surface properties are of great importance, as for example in air–sea gas transfer, wave-breaking effects should be included.

The impact of injection of turbulence into the ML from Langmuir circulation is much larger than that of wave breaking. This is principally because, unlike wave breaking where TKE input occurs just near the surface and rapidly decays with depth, TKE input from Langmuir cells occurs throughout the water column, wherever significant ambient shear stress and Stokes drift exist. The impact of including Langmuir cell terms in the ML model on the SST is rather small on diurnal time scales, but can be appreciable on seasonal time scales. OWS Papa simulations for the year 1961 showed that the SST can decrease by as much as 0.5 °C due to the additional mixing and ML deepening caused by Langmuir cells. Nevertheless, such SST changes are well within the uncertainties in modeled SST that exist simply because of our imperfect knowledge of surface heat and radiative fluxes used to drive the ML models. This may explain why the current generation mixed layer models, which ignore both wave mixing and Langmuir circulation influences, have managed to simulate the SST reasonably well, since the inevitable adjustments in surface fluxes, well within reason, may have contributed to this outcome.

To properly include the effect of Langmuir cells in the two-equation turbulence models, it is important to make the coefficient that multiplies the Langmuir production term in the length scale equation much greater than unity. Otherwise, the increase in the turbulence length scale (and hence mixing) in the mixed layer, brought on by Langmuir cells, cannot be reproduced. In one-equation turbulence models, where the length scale is prescribed, appropriate changes must be made to the prescribed length scale to reproduce Langmuir cell effects.

Acknowledgements

We acknowledge with pleasure the support by the NSF under grants ATM 9629702 and 9525847 to CAC and by the ONR under grant ONR N00014-99-1-0788 and ONR N00014-02-1-1043 to LHK. We thank an anonymous reviewer for bringing to our attention the LES calculations of Jim McWilliams and colleagues. This paper has benefited significantly from their work.

Appendix A. Comparison with analytical solutions for the wave-mixed surface layer

In an effort to compute the velocity profiles adjacent to the air–sea interface of a wave- and wind-mixed oceanic mixed layer, Craig (1996) derived an analytical expression for the TKE in the surface layer. In the current notation, it is

$$q^2 = B_1^{2/3} u_*^2 \left[1 + 3m\alpha' \kappa \left(\frac{z_0}{z_0 - z} \right)^{3m} \right]^{2/3} \tag{A.1}$$

where z_0 is the roughness scale, m is an arbitrary constant and $\alpha' u_*^3$ is the energy flux from wave breaking. Craig (1996) assumed $\ell = \kappa(z_0 - z)$ to derive this expression. This also yields the following expression for the dissipation rate:

$$\frac{\varepsilon z_0}{u_*^3} = \frac{1}{\kappa}\left(\frac{z_0}{z_0 - z}\right)\left[1 + 3m\alpha'\kappa\left(\frac{z_0}{z_0 - z}\right)^{3m}\right] \tag{A.2}$$

When the energy flux from breaking waves is zero ($\alpha' = 0$), the solution yields the log-law behavior for the dissipation rate

$$\frac{\varepsilon z_0}{u_*^3} = \frac{1}{\kappa}\left(\frac{z_0 - z}{z_0}\right)^{-1} \tag{A.3}$$

whereas, when the flux dominates, the dissipation rate becomes

$$\frac{\varepsilon z_0}{\alpha' u_*^3} = 3m\left(\frac{z_0 - z}{z_0}\right)^{-3m-1} \tag{A.4}$$

akin to that for a stirring grid. At $z = 0$, the dissipation rate is given by

$$\frac{\varepsilon z_0}{\alpha' u_*^3} = 3m + \frac{1}{\alpha'\kappa} \tag{A.5}$$

The turbulence velocity scale $q \sim [z_0/(z_0 - z)]^{-m}$ close to the surface (akin to stirring grid solution) but transitions to the log-layer behavior $q \sim u_*$ as $[z_0/(z_0 - z)] \to 0$. The transition distance is given by

$$\left(\frac{z_0}{z_0 - z}\right)_{\mathrm{t}} = (3m\alpha'\kappa)^{1/(3m)} \tag{A.6}$$

For $m = 1$, this value is about 5 (assuming $\alpha' \sim 100$). Craig's analytical solution has been used as the basis of a modification to the $k - \varepsilon$ model of turbulent mixing by Burchard (2001).

A quantity of considerable interest in geophysical boundary layers is $\Phi_{\mathrm{M}} = \frac{\ell}{u_*}\frac{\mathrm{d}U}{\mathrm{d}z}$, which is given by

$$\Phi_{\mathrm{M}} = \left[1 + \alpha'\left(\frac{3}{B_1 S_{\mathrm{q}}}\right)^{1/2}\left(\frac{z_0}{z_0 - z}\right)^{3m}\right]^{-1/3} \tag{A.7}$$

which assumes a value of 1 for the neutral log-layer and $0.246(\frac{z_0 - z}{z_0})^m$ in the wave-mixed region immediately below the interface.

As indicated earlier, there is no reason to presume $\ell = \kappa(z_0 - z)$ in the wave-mixed layer, although this law should prevail in the neutral log-layer region. In fact, assuming the proportionality constant is κ leads to very small values of S_q for values of m in the vicinity of 1 (0.125 for $m = 1$). On the other hand, the traditional value of $S_q(0.41)$ is obtained for $m = 0.57$, which is however not permissible in Eq. (4.6). Since most indications are that the value of m is close to unity, this assumption must be relaxed. Assuming instead that $\ell = b(z_0 - z)$ in the wave-mixed region, the length scale must be chosen as

$$\begin{aligned} \ell &= \kappa'(z_0 - z) \\ \kappa' &= b + (\kappa - b)\left\{1 - \exp\left[d\left(1 - \frac{z_0 - z}{z_0}\right)\right]\right\} \end{aligned} \tag{A.8}$$

This assures proper asymptotic behavior in the wave-mixed and logarithmic regions. We have introduced another arbitrary constant d, which determines how fast the transition in the value of the constant of proportionality occurs. The value of d must be determined empirically.

The non-constant value of κ' makes it necessary to modify Craig's solutions. Since in the coordinate y defined as:

$$y = \int_0^z \frac{dz'}{\ell(z')} \tag{A.9}$$

the length scale appears implicitly, the solution for q remains unchanged and is given by Eq. (15) of Craig (1996):

$$q^3 = u_*^3(B_1 + \alpha' c e^{ay}); \quad a = \left(\frac{3}{B_1 S_q}\right)^{1/2} = 3mb; \quad c = \left(\frac{3B_1}{S_q}\right)^{1/2} = 3B_1 mb \tag{A.10}$$

The various quantities can now be written as:

$$\begin{aligned}
&\frac{\mathrm{TKE}}{u_*^2} = \frac{B_1^{2/3}}{2}[1 + 3mb\alpha' e^{\mathrm{ay}}]^{2/3} \\
&\frac{\varepsilon z_0}{u_*^3} = \frac{1}{\kappa'}\left(\frac{z_0}{z_0 - z}\right)[1 + 3mb\alpha' \mathrm{e}^{ay}] \\
&\frac{K_\mathrm{M}}{u_* z_0} = \kappa'\left(\frac{z_0 - z}{z_0}\right)[1 + 3mb\alpha' \mathrm{e}^{ay}]^{1/3} \\
&\Phi_\mathrm{M} = [1 + 3mb\alpha' \mathrm{e}^{ay}]^{-1/3}
\end{aligned} \tag{A.11}$$

Note that the value of y in Eqs. (A.10) and (A.11) has to be obtained by integration of Eq. (A.9). We recover Craig's original solutions if we put $b = \kappa$ in Eq. (A.8), since Eq. (A.9) then yields $ay = (z_0/(z_0 - z)]^{\mathrm{m}}$.

The value of m can now be chosen as 1, and $b = \kappa/1.81$ in Eq. (A.11), keeping the value of S_q unchanged at 0.41. These solutions will be compared to the solutions obtained by the modified mixed layer model in Fig. 1. Note that the value of q^2 at the surface is

$$q^2 = B_1^{2/3}[1 + 3mb\alpha']^{2/3} u_*^2 \tag{A.12}$$

and the value of Φ_M at $z = 0$ is 0.246, the same value as given by the Craig (1996) solution (Eq. (A.7)), even though the variation of Φ_M with depth is no longer a simple power law.

In the constant-flux surface layer of the lower atmospheric boundary layer, quantities like Φ_M are universal functions of the Monin–Obukhoff similarity variable $\zeta = z/L$ where L is the Monin–Obukhoff length scale that denotes the relative strength of the density stratification in the surface layer. It is often presumed that the same similarity relationships hold in the OML adjacent to the air–sea interface. However, the presence of a dynamical interface with an actively breaking surface wave field is an important distinction that is very often ignored (for example, Large et al., 1994). Eq. (A.12) suggests that normalized quantities like Φ_M in the constant flux surface layer of geophysical boundary layers must be plotted against $(z - z_0)/L$, not $\zeta = z/L$. This is not of major importance in the atmospheric boundary layer, where z_0/L tends to be small, but in the oceanic mixed layer, z_0/L can be of order unity. Also, there is a small region around $\zeta = 0$, where Φ_M

increases from a value of about 0.25 at $\zeta = 0$ its canonical value of 1, the extent of this region depending very much on the value of z_0/L. In other words, the Monin–Obukhoff similarity variable is not the only parameter in the problem, and z_0/L or equivalently the wave age c_p/u_* is also important in the upper OML.

The numerical model was run with a high vertical resolution ($\Delta z = 0.1$ m) to resolve the wave-mixed layer for a neutrally stratified mixed layer driven by 0.5 N m^{-2} wind stress and fully developed waves ($c_p/u_* = 26$, $\alpha' = 100$). Both the Neumann boundary condition (TKE flux at the surface, Eq. (5.7)) and the Dirichlet boundary condition (Eq. (A.12)) were tested. Both yielded similar results, but since the Dirichlet condition is simpler to impose computationally, the model was henceforth run with it. Since the model uses a differential equation to calculate ℓ (Craig and Banner, 1994 and Stacey and Pond, 1997, prescribe an analytical form for ℓ instead), the surface boundary condition needed in the solution of the $q^2\ell$ equation (4.2) requires ℓ to be prescribed at the surface. The value of ℓ depends on the waterside roughness length about which not much is known (see the discussion by Craig and Banner, 1994; Burchard, 2001). It is however known that its value can be as much as 1 m, and from dimensional arguments, it should be similar in form to the Charnock law for the air-side roughness length, that is, it should be proportional to u_*^2/g, with the proportionality constant being perhaps fetch-dependent. Alternatively, the roughness length should be proportional to the significant wave height. For a narrow-band spectrum, the probability distribution of wave height maxima can be approximated by a Rayleigh distribution (Phillips, 1977; Kantha and Clayson, 2000) and in this case, the significant wave height H_s is equal to $4(\overline{\zeta^2})^{1/2}$. We take the roughness scale to be equal to $1.6H_s$, which is consistent with Stacey (1999), who also found that $z_0 \sim O(H_s)$. For a discussion of the parameterization of z_0, see Stacey (1999).

Fig. 7 shows normalized values of TKE, its dissipation rate, and the velocity profile from the model. It also shows these quantities without wave breaking. It can be seen that the model results

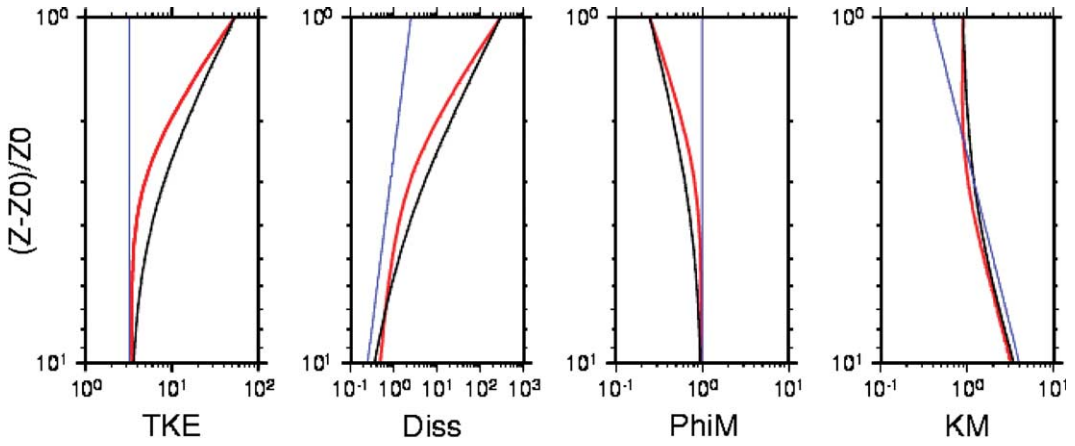

Fig. 7. Normalized TKE, TKE dissipation rate, the Monin–Obukhoff similarity function Φ_M and the eddy viscosity K_M plotted as a function of $(z_0 - z)/z_0$ for model vertical resolution Δz of 0.1 m (thick red lines). The panels show from left to right, TKE normalized by u_*^2, dissipation rate of TKE normalized by, u_*^2/z_0, Φ_M and K_M normalized by $u_* z_0$. Quantity u_* is the water-side friction velocity and z_0 is the roughness scale. Solutions without wave breaking (thin blue lines) and modified Craig (1996) analytical solutions (medium black lines) are also shown.

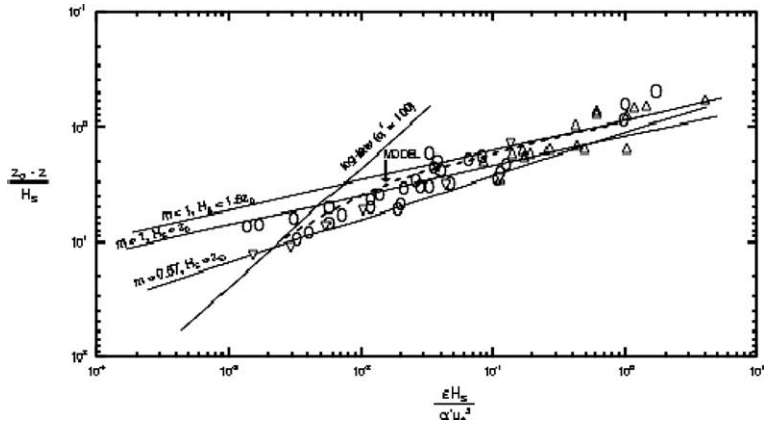

Fig. 8. Normalized dissipation rate plotted as a function of $(z_0 - z)/z_0$ and compared with measurements of Anis and Moum (1995) denoted by symbol ∇, Drennan et al. (1996) denoted by symbol Δ and Terray et al. (1996) denoted by symbol O (figure adapted from Burchard, 2001).

correspond roughly to the modified Craig solutions with $d = 0.1$, which are also shown. Changing the model resolution Δz to 0.01 and 1.0 m produced very little differences, which are not significant in light of the scatter in the observational data relevant to these parameters (for example, see Fig. 8).

Fig. 8 shows the normalized dissipation rate $\varepsilon z_0/(\alpha' u_*^3)$ plotted against the normalized distance from the surface $(z - z_0)/z_0$ from the model (assuming $\alpha' = 100$), compared against available observations. The model is within the error bars of these difficult measurements. Also shown are the analytical solutions for pure wave-breaking for values of $m = 1$ (value chosen in this paper) and $m = 0.57$ (Craig's value). The log-law behavior is also shown assuming $\alpha' = 100$. The numerical model behavior is quite acceptable.

References

Agarwal, Y.C., Terray, E.A., Donelan, M.A., Hwang, P.A., Williams III, A.J., Drennan, W.M., Kahma, K.K., Kitaigorodskii, S.A., 1992. Enhanced dissipation of kinetic energy beneath surface waves. Nature 359, 219–220.

Anis, A., Moum, J.N., 1992. The superadiabatic surface layer of the ocean during convection. J. Phys. Oceanogr. 22, 1221–1227.

Anis, A., Moum, J.N., 1995. Surface wave–turbulence interactions: scaling $\varepsilon(z)$ near the sea surface. J. Phys. Oceanogr. 25, 2025–2045.

Burchard, H., 2001. Simulating the wave-enhanced layer under breaking surface waves with two-equation turbulence models. J. Phys. Oceanogr. 31, 3133–3145.

Burchard, H., Deleersnijder, E., 2001. Investigating the stability of algebraic non-equilibrium second-moment turbulence closure models. Ocean Modeling 3, 33–50.

Clayson, C.A., Chen, A., Kantha, L.H., Webster, P.J., 1997. Numerical simulations of the equatorial Pacific during the TOGA/COARE IOP, AMS abstract. In: Proceedings of the 22nd Conference on Hurricanes and Tropical Meteorology, May 19–23, 1997, Fort Collins, C0, pp. 600–601.

Craig, P.D., 1996. Velocity profiles and surface roughness under breaking waves. J. Geophys. Res. 101, 1265–1277.

Craig, P.D., Banner, M.L., 1994. Modeling wave-enhanced turbulence in the ocean surface layer. J. Phys. Oceanogr. 24, 2546–2559.

Craik, A.D.D., Leibovich, S., 1976. A rational model for Langmuir circulation. J. Fluid Mech. 73, 401–426.

D'Alessio, J.S.D., Abdella, K., McFarlane, N.A., 1998. A new second-order turbulence closure scheme for modeling the oceanic mixed layer. J. Phys. Oceanogr. 28, 1624–1641.

Drennan, W.M., Donelan, M.A., Terray, E.A., Katsaros, K.B., 1996. Oceanic turbulence dissipation measurements in SWADE. J. Phys. Oceanogr. 26, 808–815.

Drennan, W.M., Kahma, K.K., Terray, E.A., Donelan, M.A., Kitaigorodskii, S.A., 1992. Observations of the enhancement of the kinetic energy dissipation beneath breaking wind waves. In: Banner, M.L., Grimshaw, R.H.J. (Eds.), Breaking Waves. Springer, pp. 95–101.

Farmer, D.M., Li, M., 1995. Patterns of bubble clouds organized by Langmuir circulation. J. Phys. Oceanogr., 25.

Forristall, G.Z., 1981. Measurements of a saturated range in ocean wave spectra. J. Geophys. Res. 86, 8075–8084.

Galperin, B., Kantha, L.H., Hassid, S., Rosati, A., 1988. A quasi-equilibrium turbulent energy model for geophysical flows. J. Atmos. Sci. 45, 55–62.

Gargett, A.E., 1989. Ocean turbulence. Ann. Rev. Fluid Mech. 21, 419–451.

Hopfinger, E.J., Toly, J.-A., 1976. Spatially decaying turbulence and its relation to mixing across density interfaces. J. Fluid Mech. 78, 155–175.

Kahma, K.K., 1981. A study of the growth of the wave spectrum with fetch. J. Phys. Oceanogr. 11, 1503–1515.

Kantha, L.H., 1988. On some aspects of second moment closure. Unpublished report, Geophysical Fluid Dynamics Laboratory, Princeton, NJ, p. 151.

Kantha, L.H., Rosati, A., 1990. The effect of curvature on turbulence in stratified fluids. J. Geophys. Res. 95, 20313–320330.

Kantha, L.H., Rosati, A., Galperin, B., 1989. Effect of rotation on vertical mixing and associated turbulence in stratified fluids. J. Geophys. Res. 94, 4843–4854.

Kantha, L.H., Clayson, C.A., 1994. An improved mixed layer model for geophysical applications. J. Geophys. Res. 99, 25235–25266.

Kantha, L.H., Clayson, C.A., 2000. Small Scale Processes in Geophysical Flows. Academic Press, New York, p. 888.

Kitaigorodskii, S.A., 1986. The equilibrium ranges in wind–wave spectra. In: Phillips, O.M., Hasselmann, K. (Eds.), Wave Dynamics and Radio Probing of the Ocean Surface. Plenum, New York, pp. 9–40.

Kitaigorodskii, S.A., Donelan, M.A., Lumley, J.L., Terray, E.A., 1983. Wave–turbulence interactions in the upper ocean. Part II: Statistical characteristics of wave and turbulent components of the random velocity field in the marine surface layer. J. Phys. Oceanogr. 13, 1988–1999.

Kundu, K.P., 1980. A numerical investigation of mixed-layer dynamics. J. Phys. Oceanogr. 10, 220–236.

Langmuir, I., 1938. Surface motion of water induced by wind. Science 87, 119–123.

Large, W.G., McWilliams, J.C., Doney, S.C., 1994. Oceanic mixing: a review and a model with a nonlocal boundary layer parameterization. Rev. Geophys. 32, 363–403.

Leibovich, S., 1983. The form and dynamics of Langmuir circulations. Ann. Rev. Fluid Mech. 15, 391–427.

Li, M., Garrett, C., 1993. Cell merging and the jet downwelling ratio in Langmuir circulation. J. Mar. Res. 51, 737–769.

Longuet-Higgins, M.S., 1969. On wave breaking and the equilibrium spectrum of wind-generated waves. Proc. R. Soc. A 310, 151–159.

McWilliams, J.C., Sullivan, P.P., Moeng, C.-H., 1997. Langmuir turbulence in the ocean. J. Fluid Mech. 334, 1–30.

Mellor, G.L., Yamada, T., 1974. A hierarchy of turbulence closure models for planetary boundary layers. J. Atmos. Sci. 31, 1791–1806.

Mellor, G.L., Yamada, T., 1982. Development of a turbulence closure model for geophysical fluid problems. Rev. Geophys. Space Phys. 20, 851–875.

Melville, W.K., 1994. Energy dissipation by breaking waves. J. Phys. Oceanogr. 24, 2041–2049.

Niiler, P.P., Kraus, E.B., 1977. One-dimensional models of the upper ocean. In: Kraus, E.B. (Ed.), Modelling and Prediction of the Upper Layers of the Ocean. Pergamon, New York, pp. 143–172.

Osborn, T., Farmer, D.M., Vagle, S., Thorpe, S., Cure, M., 1992. Measurements of bubble plumes and turbulence from a submarine. Atmos. Ocean 30, 419–440.

Phillips, O.M., 1958. The equilibrium range in the spectrum of wind-generated ocean waves. J. Fluid Mech. 4, 426–434.
Phillips, O.M., 1977. The Dynamics of the Upper Ocean, second ed. Cambridge University Press., p. 250.
Phillips, O.M., 1985. Spectral and statistical properties of the equilibrium range in wind-generated gravity waves. J. Fluid Mech. 156, 505–531.
Plueddemann, A.J., Smith, J.A., Farmer, D.M., Weller, R.A., Crawford, W.R., Pinkel, R., Vagle, S., Gnanadesikan, A., 1996. Structure and variability of Langmuir circulation during the Surface Wave Processes Program. J. Geophys. Res. 101, 3525–3543.
Pollard, R.T., 1977. Observations and theories of Langmuir circulations and their role in near surface mixing. In: Angel, M., (Ed.), A Voyage of Discovery: G. Deacon 70th Anniversary Volume, Pergamon Press, New York, pp. 235–251.
Rapp, R.J., Melville, W.K., 1990. Laboratory measurements of deep-water breaking waves. Phil. Trans. R. Soc. London A 331, 735–800.
Skyllingstad, E.D., Denbo, D.W., 1995. An ocean large-eddy simulation of Langmuir circulations and convection in the surface layer. J. Geophys. Res. 100, 8501–8522.
Stacey, M.W., 1999. Simulation of the wind-forced near-surface circulation in Knight Inlet: A parameterization of the roughness length. J. Phys. Oceanogr. 29, 1363–1367.
Stacey, M.W., Pond, S., 1997. On the Mellor–Yamada turbulence closure scheme: the surface boundary condition for q^2. J. Phys. Oceanogr. 27, 2081–2086.
Terray, E.A., Donelan, M.A., Agarwal, Y.C., Drennan, W.M., Kahma, K.K., Williams III, A.J., Hwang, P.A., Kitaigorodskii, S.A., 1996. Estimates of kinetic energy dissipation under breaking waves. J. Phys. Oceanogr. 26, 792–807.
Thorpe, S.A., 1984. The effect of Langmuir circulation on the distribution of submerged bubbles caused by breaking wind waves. J. Fluid Mech. 142, 151–170.
Thorpe, S.A., 1992. Bubble clouds and the dynamics of the upper ocean. Quart. J. R. Meteorol. Soc. 118, 1–22.
Toba, Y., 1973. Local balance in the air–sea boundary processes. III. On the spectrum of wind waves. J. Oceanogr. Soc. Japan 29, 209–220.
Weller, R.A., Price, J.F., 1988. Langmuir circulation within the oceanic mixed layer. Deep-Sea Res. 35, 711–747.
Weller, R.A., Donelan, M.A., Briscoe, M.G., Huang, N.E., 1991. Riding the crest: A tale of two wave experiments. Bull. Amer. Meteorol. Soc. 72, 163–183.